A Numerical Lifting-Line Method Using Horseshoe Vortex Sheets

Douglas F. Hunsaker
Utah State University

A numerical method based on the original lifting-line theory of Prandtl is developed which includes the influence of horseshoe vortex sheets. The method is an attempt at developing a higher-order method than previous delta-function methods of the same type. The definition of a horseshoe vortex sheet singularity is introduced and the velocity induced at an arbitrary point in space by the singularity is developed. No closed-form solution for this induced velocity was found for points not collinear with the bound portion of the singularity. Additionally, the velocity induced along the bound portion of a horseshoe vortex sheet with sweep is indeterminate. The singularity was used to develop a numerical method capable of predicting the aerodynamic forces and moments on a system of lifting surfaces. The method gives results within the accuracy of other similar methods, but requires higher grid refinement and more computation than previous methods.

I. Introduction

PRANDTL'S classical lifting-line theory[1,2] has had a profound effect on aerodynamics up to this point in time. In the development of his theory, Prandtl related the two-dimensional airfoil lift at each section of the wing to the local circulation through the two-dimensional vortex lifting law[3,4]. This method has been found to be very accurate for wings with aspect ratios greater than about 4. However, it is limited in its application to wings with no sweep and no dihedral. Additionally, Prandtl's classical development does not account for the interaction of multiple lifting surfaces.

Several numerical methods rooted in this original theory can be found in the literature[5,6,7]. These methods have been developed to extend the original theoretical basis of Prandtl's theory to wings with sweep and dihedral and to model the interaction of multiple lifting surfaces. However, some of the most common methods cannot be considered a direct numerical analogy to the original theory of Prandtl. Perhaps the most well-known numerical method that fits into this category is that presented by Katz and Plotkin[7]. Although the method presented by Katz and Plotkin is often referred to as the lifting-line method, it could more appropriately be referred to as a vortex lattice method applied using only a single element in the chordwise direction. This title may be more appropriate because rather than closing the system of equations by relating the circulation at each section to the two-dimensional section lift, a closing boundary condition is implemented requiring the normal velocity at the three-quarter chord to be zero.

Phillips and Snyder[8] presented a numerical equivalent of Prandtl's original lifting-line method which can be used to evaluate the flow about wings with sweep and dihedral. This development is a more rigorous equivalent to Prandtl's original theory because the relationship between the two-dimensional airfoil lift at each section of the wing and the three-dimensional vortex lifting law[9] is used to obtain the local circulation at each wing section. This method shows promising potential for both the aircraft industry and the wind and water turbine industries where lifting surfaces conventionally have aspect ratios greater than 4. Additionally, the method can easily be extended to allow for trailing vortex movement and rollup behind the lifting surface and thus account for both non-rotating and rotating flows. According to Phillips and Snyder, this method accurately predicts the lift coefficient for wings with sweep and dihedral and requires only a fraction of the cost of conventional computational fluid dynamics (CFD) methods to obtain grid-converged results.

In traditional numerical lifting-line methods, a system of lifting surfaces is synthesized by discretizing the wing into a series of horseshoe vortices, each having a strength equivalent to the bound vorticity at the location of the section. This is convenient because according to the Helmholz vortex lifting law, vorticity cannot be produced in a potential flowfield, and a vortex cannot begin or end in the flowfield. Therefore, horseshoe vortices are often used which extend from an infinite distance downstream, across a bound portion of the wing, and then an infinite distance back downstream. Because each horseshoe vortex has a discrete value and the vorticity at every other point in the flow not occupied by a segment of the vortex is zero, this approach creates a vorticity field synthesized by a series of delta functions. Other delta function type methods include the vortex ring method equivalent to the doublet panel method for 3D flows. These vortices are arranged in rings of constant strength which satisfies the Helmholz vortex law. A numerical method based on delta function singularities is often referred to as a zeroth-order method.

A first-order method can be developed by replacing the discrete horseshoe vortices with horseshoe vortex sheets of constant strength. Such an approach allows vorticity to continuously be shed from the wing, rather than discretely as is the case with traditional methods. This paper presents such a method.

II. The Horseshoe Vortex Sheet

A horseshoe vortex sheet is composed of two semi-infinite trailing vortex segments connected by one bound vortex segment of finite length and one semi-infinite vortex sheet as shown in Fig. 1. The semi-infinite vortex segments have strengths Γ_a and Γ_b that in general will differ from each other but are constant along their respective lengths. They are connected by the bound vortex segment which varies linearly in strength along its length beginning at $\Gamma = \Gamma_a$ and ending at $\Gamma = \Gamma_b$. These three vortex segments form the outline of a trailing vortex sheet of constant strength. The velocity induced at an arbitrary point **P** in space by the entire horseshoe vortex sheet is the sum of the velocity induced by the two trailing vortex segments, the bound vortex segment, and the vortex sheet

$$\mathbf{V} = \mathbf{V}_t + \mathbf{V}_l + \mathbf{V}_s \tag{1}$$

Here $\mathbf{V}_t$ is the velocity induced by the two trailing vortex segments, $\mathbf{V}_l$ is the velocity induced by the bound vortex segment, and $\mathbf{V}_s$ is the velocity induced by the trailing vortex sheet.

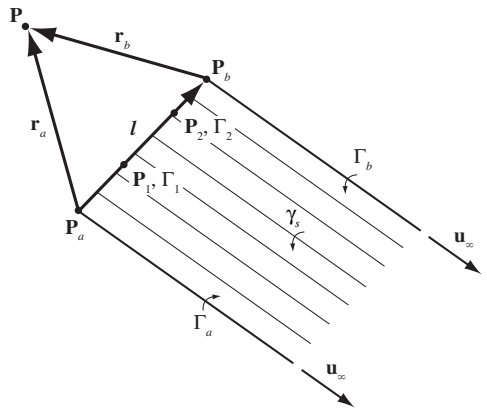

Figure 1. Position vectors and geometry for a horseshoe vortex sheet.

A. Semi-Infinite Vortex Segments of Constant Strength

The horseshoe vortex sheet includes two semi-infinite trailing vortices that extend from points $\mathbf{P}_a$ and $\mathbf{P}_b$ to infinity in the direction of the freestream. The velocity induced by the trailing vortex segments is developed by Phillips and Snyder[8] and can be written as

$$\mathbf{V}_t = \frac{1}{4\pi}\left[-\frac{\Gamma_a(\mathbf{u}_\infty \times \mathbf{r}_a)}{r_a(r_a - \mathbf{u}_\infty \cdot \mathbf{r}_a)} + \frac{\Gamma_b(\mathbf{u}_\infty \times \mathbf{r}_b)}{r_b(r_b - \mathbf{u}_\infty \cdot \mathbf{r}_b)}\right] \tag{2}$$

B. Vortex Line Segment with Linearly Varying Strength

The bound portion of the horseshoe vortex sheet is a vortex line segment with linearly varying strength beginning at point $\mathbf{P}_a$ with strength Γ_a and ending at point $\mathbf{P}_b$ with vortex strength Γ_b. The geometry for this vortex line segment is shown in Fig. 2. The differential velocity induced by a differential directional vortex segment of length $\mathbf{d}\boldsymbol{l}$ is

$$\mathbf{dV}_l = \frac{\Gamma \mathbf{d}\boldsymbol{l} \times \mathbf{r}}{4\pi|\mathbf{r}|^3} \tag{3}$$

Introducing ζ as a dimensionless distance along the line segment $\boldsymbol{l}$ gives the change of variables

$$\mathbf{d}\boldsymbol{l} \equiv \boldsymbol{l} d\zeta \tag{4}$$

The use of ζ in the geometry gives the relations

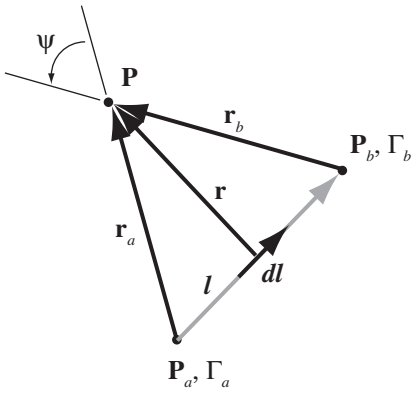

Figure 2. Position vectors showing the geometry for a vortex line segment with varying strength.

$$\mathbf{r} = \mathbf{r}_a - \zeta \boldsymbol{l} \tag{5}$$

$$\mathbf{d}\boldsymbol{l} \times \mathbf{r} = \boldsymbol{l} d\zeta \times (\mathbf{r}_a - \zeta \boldsymbol{l}) = \boldsymbol{l} \times \mathbf{r}_a d\zeta \tag{6}$$

$$|\mathbf{r}|^3 = (r_a^2 - 2\boldsymbol{l} \cdot \mathbf{r}_a \zeta + l^2 \zeta^2)^{3/2} \tag{7}$$

and the local vortex filament strength is a linear function which can be expressed as

$$\Gamma = \Gamma_a + (\Gamma_b - \Gamma_a)\zeta \tag{8}$$

Using Eqs. (4) – (8) in Eq. (3) gives

$$\mathbf{dV}_l = \frac{\Gamma \mathbf{d}\boldsymbol{l} \times \mathbf{r}}{4\pi|\mathbf{r}|^3} = \frac{[\Gamma_a + (\Gamma_b - \Gamma_a)\zeta]\boldsymbol{l} \times \mathbf{r}_a d\zeta}{4\pi(r_a^2 - 2\boldsymbol{l} \cdot \mathbf{r}_a \zeta + l^2 \zeta^2)^{3/2}} \tag{9}$$

The total velocity induced by the entire line segment is

$$\mathbf{V}_l = \frac{\boldsymbol{l}\times\mathbf{r}_a}{4\pi}\int_{\zeta=0}^{1}\frac{\Gamma_a+(\Gamma_b-\Gamma_a)\zeta}{(l^2\zeta^2-2\boldsymbol{l}\cdot\mathbf{r}_a\zeta+r_a^2)^{3/2}}d\zeta \quad (10)$$

This can be integrated to yield

$$\mathbf{V}_l = \frac{\boldsymbol{l}\times\mathbf{r}_a}{4\pi[l^2r_a^2-(\boldsymbol{l}\cdot\mathbf{r}_a)^2]}\left(\frac{[-\Gamma_a\boldsymbol{l}-(\Gamma_b-\Gamma_a)\mathbf{r}_a]\cdot[\mathbf{r}_a-\boldsymbol{l}]}{[(\mathbf{r}_a-\boldsymbol{l})\cdot(\mathbf{r}_a-\boldsymbol{l})]^{1/2}} + \frac{\boldsymbol{l}\cdot\mathbf{r}_a\Gamma_a+r_a^2(\Gamma_b-\Gamma_a)}{r_a}\right) \quad (11)$$

By definition of the geometry,

$$\boldsymbol{l} = \mathbf{r}_a - \mathbf{r}_b \quad (12)$$

which gives the relations

$$l^2r_a^2-(\boldsymbol{l}\cdot\mathbf{r}_a)^2 = r_a^2r_b^2-(\mathbf{r}_a\cdot\mathbf{r}_b)^2 \quad (13)$$

$$\boldsymbol{l}\times\mathbf{r}_a = \mathbf{r}_a\times\mathbf{r}_b \quad (14)$$

Using Eqs. (12) – (14) in Eq. (11) yields

$$\mathbf{V}_l = \frac{1}{4\pi}\frac{\mathbf{r}_a\times\mathbf{r}_b}{r_a^2r_b^2-(\mathbf{r}_a\cdot\mathbf{r}_b)^2}\left[\Gamma_a\boldsymbol{l}\cdot\left(\frac{\mathbf{r}_a}{r_a}-\frac{\mathbf{r}_b}{r_b}\right) + (\Gamma_b-\Gamma_a)\left(r_a-\frac{\mathbf{r}_a\cdot\mathbf{r}_b}{r_b}\right)\right] \quad (15)$$

Applying trigonometric identities, the relationship can be developed

$$\begin{aligned} r_a^2r_b^2-(\mathbf{r}_a\cdot\mathbf{r}_b)^2 &= r_a^2r_b^2(1-\cos^2\psi) \\ &= r_a^2r_b^2\sin^2\psi = |\mathbf{r}_a\times\mathbf{r}_b|^2 \end{aligned} \quad (16)$$

Using Eq. (16) in Eq. (15) and simplifying yields a useful expression for the velocity induced by a vortex line segment with linearly varying strength

$$\mathbf{V}_l = \frac{1}{4\pi}\frac{(\Gamma_br_a+\Gamma_ar_b)(\mathbf{r}_a\times\mathbf{r}_b)}{r_ar_b(r_ar_b+\mathbf{r}_a\cdot\mathbf{r}_b)} \quad (17)$$

Notice that this expression is only indeterminate when the angle between $\mathbf{r}_a$ and $\mathbf{r}_b$ is $\pm\pi$. It is not indeterminate when the angle between $\mathbf{r}_a$ and $\mathbf{r}_b$ is zero.

C. Semi-Infinite Vortex Sheet with Constant Strength

The bound and trailing segments of the horseshoe vortex sheet form the outline of the trailing vortex sheet. The geometry for a semi-infinite vortex sheet with constant strength is shown in Fig. 3.

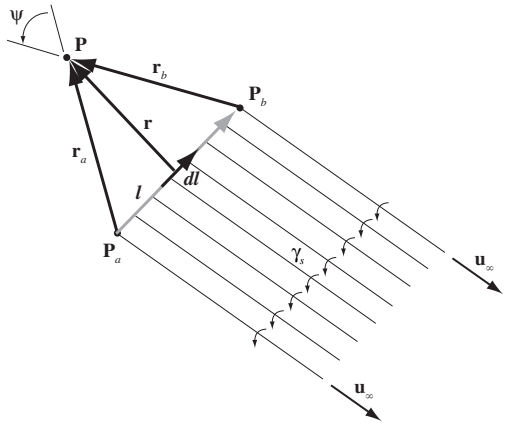

Figure 3. Position vectors showing the geometry for a semi-infinite vortex sheet with constant strength.

The velocity induced at a point by a single semi-infinite vortex is given by Phillips and Snyder[8]

$$\mathbf{V} = \frac{\Gamma}{4\pi}\frac{\mathbf{u}_\infty\times\mathbf{r}}{r(r-\mathbf{u}_\infty\cdot\mathbf{r})} \quad (18)$$

where $\mathbf{r}$ is the vector from the beginning point of the semi-infinite vortex to the point of interest. A semi-infinite vortex sheet is composed of a continuous sheet of semi-infinite vortices beginning along the vector $\boldsymbol{l}$ and extending infinitely along the unit vector $\mathbf{u}_\infty$ and having a strength per unit length along $\boldsymbol{l}$ of γ_s. A differential segment of the vortex sheet having a length of dl in the direction of $\boldsymbol{l}$ induces a differential velocity of

$$d\mathbf{V}_s = \frac{\gamma_s dl}{4\pi}\frac{\mathbf{u}_\infty\times\mathbf{r}}{r(r-\mathbf{u}_\infty\cdot\mathbf{r})} \quad (19)$$

Again, defining ζ as a dimensionless distance along the line segment $\boldsymbol{l}$ gives the change of variables

$$dl = ld\zeta \quad (20)$$

Using ζ in the geometry definitions gives

$$\mathbf{r} = \mathbf{r}_a - \zeta\boldsymbol{l} \quad (21)$$

which gives the relation

$$r = |\mathbf{r}| = (r_a^2-2\boldsymbol{l}\cdot\mathbf{r}_a\zeta+l^2\zeta^2)^{1/2} \quad (22)$$

Using Eqs. (20) – (22) in Eq. (19) gives

$$d\mathbf{V}_s = \frac{\gamma_s l}{4\pi}\frac{(\mathbf{u}_\infty\times\mathbf{r}_a)-\zeta(\mathbf{u}_\infty\times\boldsymbol{l})}{r^2-r[\mathbf{u}_\infty\cdot\mathbf{r}_a-\zeta(\mathbf{u}_\infty\cdot\boldsymbol{l})]}d\zeta \quad (23)$$

The integral of Eq. (23) gives the total induced velocity from a semi-infinite vortex sheet of constant strength

$$\mathbf{V}_s = \frac{\gamma_s l}{4\pi} \int_{\zeta=0}^{1} \frac{(\mathbf{u}_\infty \times \mathbf{r}_a) - \zeta(\mathbf{u}_\infty \times \boldsymbol{l})}{r^2 - r[\mathbf{u}_\infty \cdot \mathbf{r}_a - \zeta(\mathbf{u}_\infty \cdot \boldsymbol{l})]} d\zeta \qquad (24)$$

The strength of the vortex sheet is related to the change in vorticity across the bound portion of the horseshoe vortex sheet according to

$$\gamma_s = -\frac{d\Gamma}{dl} = \frac{\Gamma_a - \Gamma_b}{l} \qquad (25)$$

Using Eq. (25) in Eq. (24) gives

$$\mathbf{V}_s = \frac{\mathbf{v}_s}{4\pi}(\Gamma_a - \Gamma_b) \qquad (26)$$

where

$$\mathbf{v}_s \equiv \int_{\zeta=0}^{1} \frac{(\mathbf{u}_\infty \times \mathbf{r}_a) - \zeta(\mathbf{u}_\infty \times \boldsymbol{l})}{r^2 - r[\mathbf{u}_\infty \cdot \mathbf{r}_a - \zeta(\mathbf{u}_\infty \cdot \boldsymbol{l})]} d\zeta \qquad (27)$$

is the directional vector for velocity induced by the vortex sheet at the point of interest and r is given in Eq. (22).

In general, Eq. (27) must be numerically integrated in order to evaluate the influence of the vortex sheet on an arbitrary point of interest. However, if the point of interest lies along the same line as $\boldsymbol{l}$, this integral can be evaluated differently as shown in the following two cases.

1. Case 1: A Collinear Point Not Coincident with the Vortex Sheet

For the special case of $\mathbf{r}_a = \xi \boldsymbol{l}$, Eq. (27) can be analytically integrated to yield

$$\begin{aligned} \mathbf{v}_s &= \frac{(\mathbf{u}_\infty \times \boldsymbol{l})}{[l^2 - l(\mathbf{u}_\infty \cdot \boldsymbol{l})]} \int_{\zeta=0}^{1} \frac{1}{(\xi - \zeta)} d\zeta \\ &= \begin{cases} \dfrac{(\mathbf{u}_\infty \times \boldsymbol{l})}{[l^2 + l(\mathbf{u}_\infty \cdot \boldsymbol{l})]} \ln\left(\dfrac{\xi}{\xi - 1}\right), & \xi < 0 \\ \dfrac{(\mathbf{u}_\infty \times \boldsymbol{l})}{[l^2 - l(\mathbf{u}_\infty \cdot \boldsymbol{l})]} \ln\left(\dfrac{\xi}{\xi - 1}\right), & \xi > 1 \end{cases} \end{aligned} \qquad (28)$$

Note that this solution is only good for $\xi < 0$ or $\xi > 1$. In other words, this solution is only valid for points not directly on the vortex sheet. We see from this result that if the point of interest lies along $\boldsymbol{l}$ but not directly on the line segment $\boldsymbol{l}$ itself, the integral yields a simple expression. However, if the point of interest lies directly on the line segment $\boldsymbol{l}$, this analytical expression cannot be used. Also note that this expression is valid independent of the orientation of the vortex sheet relative to the freestream. Therefore, this expression can be used for wings with sweep and dihedral.

2. Case 2: A Collinear Point Coincident with the Vortex Sheet

Several attempts were made to develop an expression for the case of $\mathbf{r}_a = \xi \boldsymbol{l}$ where $0 \le \xi \le 1$. This is the case for the velocity induced at a point lying directly on the bound portion of a vortex sheet by the vortex sheet itself. The most promising attempt, however, came from numerical results.

Using fourth-order Runge-Kutta integration, Eq. (27) was evaluated across the range of $0 \le \xi \le 1$ for several vortex sheet sweep angles each with unit length, l=1. The only modification to the standard integration routine was that the inside of the integrand was ignored when $\zeta = \xi$. This is justified on the grounds that a vortex segment does not induce any velocity at any point along its length. The integral was evaluated using coarse, medium, fine, and very fine integration step sizes of 1/100, 1/200, 1/400, and 1/800 respectively. Figure 4 shows the integration results for the magnitude of Eq. (27) as a function of ξ for sweep angles of -10.0, 0.0, 10.0, and 25.0 degrees. The large symbols represent the results of the coarse step size, the next largest represent the results of the medium step size, and on down to the small symbols which represent the results of the very fine step size.

Notice that the results converge only for the case of no sweep. This shows that if $\boldsymbol{l}$ is not perpendicular to $\mathbf{u}_\infty$, the induced velocity does not converge. This makes sense because for the case of no sweep, at a given position, ξ, the influence from the vortex segments at $+d\zeta$ and $-d\zeta$ will perfectly cancel. However, if $\boldsymbol{l}$ is not perpendicular to $\mathbf{u}_\infty$, the influence from the vortex segments at $+d\zeta$ and $-d\zeta$ will not perfectly cancel. As the numerical integration is refined, the velocity induced along the bound portion of a vortex sheet with sweep approaches infinity. Also note from Fig. 4 that the velocity induced at the corner points of the vortex sheet are indeterminate regardless of the sweep angle.

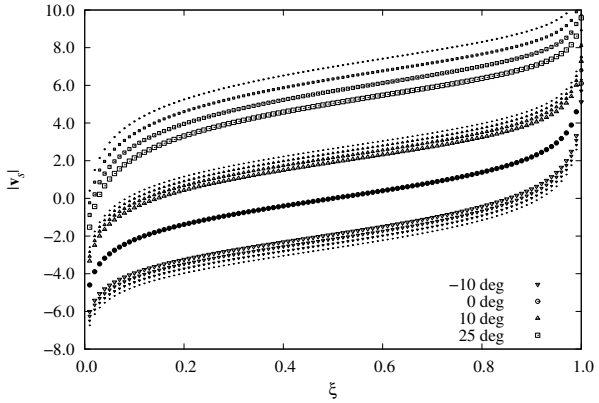

Figure 4. Magnitude of induced velocity along the bound portion of a vortex sheet.

We see from the results presented here, that the influence of a vortex sheet can only be evaluated along the bound portion of the vortex sheet if the sheet is perpendicular to the freestream velocity. Therefore, the results of the lifting-line algorithm included in this work can only be expected to be accurate for wings with no sweep and dihedral and at zero sideslip angle. An analytical approximation that can be used in place of Eq. (27) for the influence of a vortex sheet with no sweep or dihedral along the bound portion of the sheet is

$$\mathbf{v}_s = -2(.787)\frac{(\mathbf{u}_\infty \times \boldsymbol{l})}{[l^2 - l(\mathbf{u}_\infty \cdot \boldsymbol{l})]} \cdot \sinh\left\{1.24\left[\cos^{-1}(2\xi - 1) - \frac{\pi}{2}\right]\right\} \quad 0 < \xi < 1 \tag{29}$$

Figure 5 shows the magnitude of $\mathbf{v}_s$ as a function of ξ for a vortex sheet of length l=2.0 evaluated by numerically integrating Eq. (27) using a grid-resolved step size of 1/800. The analytical result of Eq. (28) and the approximation given in Eq. (29) are also included for comparison. The results show that Eq. (28) is valid for $\xi < 0$ or $\xi > 1$ for any sweep angle, and Eq. (29) is appropriate for $0 \le \xi \le 1$ when the sweep angle is zero.

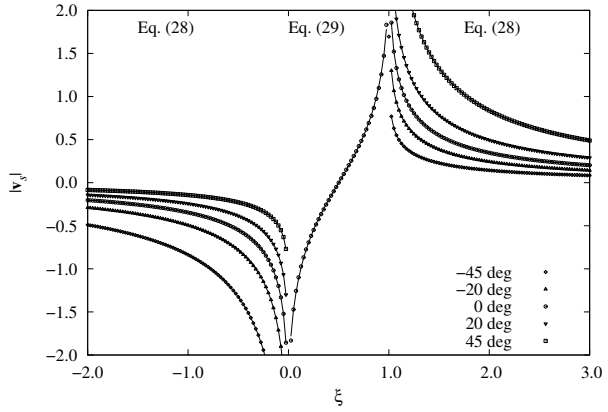

Figure 5. Magnitude of induced velocity along points collinear with the bound portion of the vortex sheet.

D. The Complete Horseshoe Vortex Sheet

The velocity induced at an arbitrary point by a complete horseshoe vortex sheet is the sum of Eqs. (2), (17), and (26)

$$\mathbf{V} = \frac{\Gamma_a}{4\pi}\left[\frac{(\mathbf{r}_a \times \mathbf{r}_b)}{r_a(r_a r_b + \mathbf{r}_a \cdot \mathbf{r}_b)} - \frac{(\mathbf{u}_\infty \times \mathbf{r}_a)}{r_a(r_a - \mathbf{u}_\infty \cdot \mathbf{r}_a)} + \mathbf{v}_s\right] + \frac{\Gamma_b}{4\pi}\left[\frac{(\mathbf{r}_a \times \mathbf{r}_b)}{r_b(r_a r_b + \mathbf{r}_a \cdot \mathbf{r}_b)} + \frac{(\mathbf{u}_\infty \times \mathbf{r}_b)}{r_b(r_b - \mathbf{u}_\infty \cdot \mathbf{r}_b)} - \mathbf{v}_s\right] \tag{30}$$

where $\mathbf{v}_s$ can be evaluated from either Eq. (27), (28), or (29) depending on the case.

III. Algorithm Formulation

A system of lifting surfaces is synthesized by discretizing the lifting surfaces into a series of horseshoe vortex sheets as shown in Fig. 6. A series of horseshoe vortex sheets is placed along the wing, the right corner of one sheet coincident with the left corner of the next sheet. The bound segment of each horseshoe vortex sheet is placed along the local quarter-chord, and is therefore aligned with the local sweep and dihedral. The trailing vortices and sheet are aligned with the freestream velocity vector, the left-corner trailing vortex extending from infinity to the quarter-chord, and the right-hand trailing vortex extending from the quarter-chord to infinity. Because the trailing vortices coincident at connecting horseshoe vortex sheets are in opposite directions, if the strength at the right corner of one horseshoe vortex sheet is identical to the strength at the left corner of the next horseshoe vortex sheet, they cancel exactly and the net shed vorticity at that point is zero except for the vorticity shed through the trailing vortex sheets.

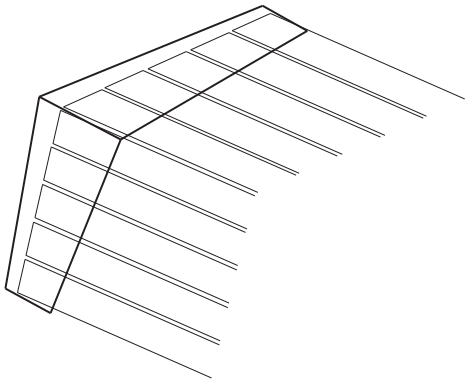

Figure 6. Horseshoe vortex sheet distribution along quarter chord of lifting surfaces.

Because the vortex sheet has constant strength, the vorticity along the bound portion of the horseshoe vortex sheet must vary linearly. In order to specify the linear change in bound vorticity, two control points are specified along the bound vortex. These are denoted as $\mathbf{P}_1$ and $\mathbf{P}_2$ and shown in Fig. 1. Here we define the relative positions of the control points to the end points of the horseshoe vortex sheet according to

$$\sigma_1 \equiv \frac{|\mathbf{P}_1 - \mathbf{P}_a|}{|\boldsymbol{l}|} \qquad \sigma_2 \equiv \frac{|\mathbf{P}_2 - \mathbf{P}_a|}{|\boldsymbol{l}|} \tag{31}$$

Cosine clustering[8] is used for the discretization of the wing into a series of horseshoe vortex sheets. Additionally, the control points are cosine clustered such that each horseshoe vortex sheet contains two control points, and each control point is evenly spaced in the cosine domain relative to the other control points. The strength of the bound vortex at the corners $\mathbf{P}_a$ and $\mathbf{P}_b$ can be related to the strength of the bound vortex at control points $\mathbf{P}_1$ and $\mathbf{P}_2$ according to

$$\begin{aligned}\Gamma_a &= \Gamma_1\left(1+\frac{\sigma_1}{\sigma_2-\sigma_1}\right)-\Gamma_2\left(\frac{\sigma_1}{\sigma_2-\sigma_1}\right)\\ \Gamma_b &= \Gamma_1\left(1-\frac{1-\sigma_1}{\sigma_2-\sigma_1}\right)+\Gamma_2\left(\frac{1-\sigma_1}{\sigma_2-\sigma_1}\right)\end{aligned} \tag{32}$$

Using Eq. (32) in Eq. (30) and rearranging gives

$$\begin{aligned}\mathbf{V} = \Gamma_1&\left[\left(1+\frac{\sigma_1}{\sigma_2-\sigma_1}\right)\mathbf{v}_a+\left(1-\frac{1-\sigma_1}{\sigma_2-\sigma_1}\right)\mathbf{v}_b\right]\\ &+\Gamma_2\left[\left(\frac{1-\sigma_1}{\sigma_2-\sigma_1}\right)\mathbf{v}_b-\left(\frac{\sigma_1}{\sigma_2-\sigma_1}\right)\mathbf{v}_a\right]\end{aligned} \tag{33}$$

where

$$\begin{aligned}\mathbf{v}_a &\equiv \frac{1}{4\pi}\left[\frac{(\mathbf{r}_a\times\mathbf{r}_b)}{r_a(r_a r_b+\mathbf{r}_a\cdot\mathbf{r}_b)}-\frac{(\mathbf{u}_\infty\times\mathbf{r}_a)}{r_a(r_a-\mathbf{u}_\infty\cdot\mathbf{r}_a)}+\mathbf{v}_s\right]\\ \mathbf{v}_b &\equiv \frac{1}{4\pi}\left[\frac{(\mathbf{r}_a\times\mathbf{r}_b)}{r_b(r_a r_b+\mathbf{r}_a\cdot\mathbf{r}_b)}+\frac{(\mathbf{u}_\infty\times\mathbf{r}_b)}{r_b(r_b-\mathbf{u}_\infty\cdot\mathbf{r}_b)}-\mathbf{v}_s\right]\end{aligned} \tag{34}$$

For each horseshoe vortex sheet, there are two unknowns, Γ_1 and Γ_2, which represent the strength of the vortex at the control points of the horseshoe vortex sheet. These vortex strengths are not known a priori and must be found by applying some constraining condition that will result in a system of equations that can be solved for the vortex strengths. If the system of lifting surfaces is discretized into n horseshoe vortex sheets, this system will have $2n$ unknowns. Therefore, a system of $2n$ equations must be developed to solve for the $2n$ unknowns. This is accomplished through the application of Prandtl's lifting-line hypothesis at the two control points placed along the bound portion of each horseshoe vortex sheet.

Prandtl's lifting-line hypothesis is based on the assumption that each spanwise segment of the lifting surface has a local lift coefficient equal to a two-dimensional segment of an infinite wing at the same angle of attack. The vortex lifting law applied to a differential segment of lifting surface gives

$$\mathbf{dF} = \rho\Gamma\mathbf{V}\times\mathbf{d}\boldsymbol{l} \tag{35}$$

This equation can be applied twice to each horseshoe vortex sheet, once at each control point of the sheet. These two points on the horseshoe vortex sheet will be referred to as the "odd" and "even" control points. Because there are n horseshoe vortex sheets, there are $2n$ control points. The local velocity at any control point, i, is the sum of the freestream velocity and the velocity induced by each vortex strength, Γ_j

$$\mathbf{V}_i = \mathbf{V}_\infty + \sum_{j=1}^{2n}\frac{\Gamma_j\mathbf{v}_{ji}}{c_j} \tag{36}$$

where

$$\mathbf{v}_{ji} \equiv c_j\begin{cases}\left[\left(1+\dfrac{\sigma_{1_k}}{\sigma_{2_k}-\sigma_{1_k}}\right)\mathbf{v}_{a_{ki}}+\left(1-\dfrac{1-\sigma_{1_k}}{\sigma_{2_k}-\sigma_{1_k}}\right)\mathbf{v}_{b_{ki}}\right], & k=\dfrac{(j+1)}{2},\quad j=\text{odd}\\ \left[\left(\dfrac{1-\sigma_{1_k}}{\sigma_{2_k}-\sigma_{1_k}}\right)\mathbf{v}_{b_{ki}}-\left(\dfrac{\sigma_{1_k}}{\sigma_{2_k}-\sigma_{1_k}}\right)\mathbf{v}_{a_{ki}}\right], & k=\dfrac{j}{2},\qquad j=\text{even}\end{cases} \tag{37}$$

is the nondimensional influence vector of the vortex strength j, which is a part of the horseshoe vortex sheet k, on control point i,

$$\begin{aligned}\mathbf{v}_{a_{ki}} &\equiv \frac{1}{4\pi}\left[\frac{(\mathbf{r}_{a_{ki}}\times\mathbf{r}_{b_{ki}})}{r_{a_{ki}}(r_{a_{ki}}r_{b_{ki}}+\mathbf{r}_{a_{ki}}\cdot\mathbf{r}_{b_{ki}})}-\frac{(\mathbf{u}_\infty\times\mathbf{r}_{a_{ki}})}{r_{a_{ki}}(r_{a_{ki}}-\mathbf{u}_\infty\cdot\mathbf{r}_{a_{ki}})}+\mathbf{v}_{s_{ki}}\right]\\ \mathbf{v}_{b_{ki}} &\equiv \frac{1}{4\pi}\left[\frac{(\mathbf{r}_{a_{ki}}\times\mathbf{r}_{b_{ki}})}{r_{b_{ki}}(r_{a_{ki}}r_{b_{ki}}+\mathbf{r}_{a_{ki}}\cdot\mathbf{r}_{b_{ki}})}+\frac{(\mathbf{u}_\infty\times\mathbf{r}_{b_{ki}})}{r_{b_{ki}}(r_{b_{ki}}-\mathbf{u}_\infty\cdot\mathbf{r}_{b_{ki}})}-\mathbf{v}_{s_{ki}}\right]\\ \mathbf{v}_{s_{ki}} &\equiv \int_{\zeta=0}^{1}\frac{(\mathbf{u}_\infty\times\mathbf{r}_{a_{ki}})-\zeta(\mathbf{u}_\infty\times\boldsymbol{l}_k)}{r_{ki}^2-r_{ki}[\mathbf{u}_\infty\cdot\mathbf{r}_{a_{ki}}-\zeta(\mathbf{u}_\infty\cdot\boldsymbol{l}_k)]}d\zeta\\ r_{ki} &\equiv (r_{a_{ki}}^2-2\boldsymbol{l}_k\cdot\mathbf{r}_{a_{ki}}\zeta+l_k^2\zeta^2)^{1/2}\end{aligned} \tag{38}$$

$\mathbf{r}_{a_{ki}}$ is the vector from corner a of the horseshoe vortex sheet k to control point i, $\mathbf{r}_{b_{ki}}$ is the vector from corner b of the horseshoe vortex sheet k to control point i, and c_j is the chord length at control point j.

Combining Eqs. (36) and (35), the differential force at control point, i, can be written as

$$\mathbf{dF}_i = \rho\Gamma_i\left(\mathbf{V}_\infty + \sum_{j=1}^{2n}\frac{\Gamma_j\mathbf{v}_{ji}}{c_j}\right)\times\mathbf{dl}_i \tag{39}$$

Using Prandtl's lifting line theory, the magnitude of this differential force must be equal to the magnitude of the two-dimensional differential segment at the same local angle of attack

$$\left|\mathbf{dF}_i\right| = \frac{1}{2}\rho V_\infty^2\widetilde{C}_{Li}(\alpha_i,\delta_i)db_ic_i \tag{40}$$

where the local angle of attack is

$$\alpha_i = \tan^{-1}\left(\frac{\mathbf{V}_i\cdot\mathbf{u}_{ni}}{\mathbf{V}_i\cdot\mathbf{u}_{ai}}\right) \tag{41}$$

and the local velocity at control point *i* is

$$\mathbf{V}_i \equiv \mathbf{V}_\infty + \sum_{j=1}^{2n}\frac{\Gamma_j\mathbf{v}_{ji}}{c_j} \tag{42}$$

Equating the magnitudes of Eqs. (39) and (40) gives

$$\left|\left(\mathbf{V}_\infty + \sum_{j=1}^{2n}\frac{\Gamma_j\mathbf{v}_{ji}}{c_j}\right)\times\mathbf{dl}_i\right|\Gamma_i - \frac{1}{2}V_\infty^2\widetilde{C}_{Li}(\alpha_i,\delta_i)db_ic_i = 0 \tag{43}$$

The differential length along the bound vortex dl_i is related to the differential segment span db_i through the local sweep angle Λ_i according to the relation

$$\cos\Lambda_i = \frac{db_i}{dl_i} \tag{44}$$

Defining the dimensionless parameters

$$\boldsymbol{\zeta}_i \equiv \frac{1}{\cos\Lambda_i}\frac{\mathbf{dl}_i}{dl_i},\quad G_i \equiv \frac{\Gamma_i}{c_iV_\infty},\quad \mathbf{u}_\infty \equiv \frac{\mathbf{V}_\infty}{V_\infty} \tag{45}$$

the formulation can be written in nondimensional form as

$$2\left|\left(\mathbf{u}_\infty + \sum_{j=1}^{2n}G_j\mathbf{v}_{ji}\right)\times\boldsymbol{\zeta}_i\right|G_i - \widetilde{C}_{Li}(\alpha_i,\delta_i) = 0 \tag{46}$$

and the local angle of attack can be written as

$$\alpha_i = \tan^{-1}\left[\frac{\mathbf{u}_i\cdot\mathbf{u}_{ni}}{\mathbf{u}_i\cdot\mathbf{u}_{ai}}\right] \tag{47}$$

where the nondimensional local velocity at control point *i* is

$$\mathbf{u}_i \equiv \mathbf{u}_\infty + \sum_{j=1}^{2n}G_j\mathbf{v}_{ji} \tag{48}$$

Applying Eq. (46) at each of the 2*n* control points provides 2*n* nonlinear independent equations. We wish to solve this system of equations using Newton's method. The system of equations can be written in compact form of

$$F(\mathbf{G}) = \mathbf{R} \tag{49}$$

where

$$F_i(\mathbf{G}) = 2\left|\left(\mathbf{u}_\infty + \sum_{j=1}^{2n}G_j\mathbf{v}_{ji}\right)\times\boldsymbol{\zeta}_i\right|G_i - \widetilde{C}_{Li}(\alpha_i,\delta_i) \tag{50}$$

and **R** is the vector of residuals which represents the error of the solution. The change in the vector of vortex strengths, **G**, which will decrease the vector of residuals can be computed from the system

$$[\mathbf{J}]\Delta\mathbf{G} = -\mathbf{R} \tag{51}$$

where [**J**] is the Jacobian matrix of partial derivatives. The Jacobian matrix can be analytically obtained and written as

$$J_{ij} = \frac{\partial F_i}{\partial\Gamma_j} = \delta_{ij}2\left|\mathbf{w}_i\right| + \frac{2\mathbf{w}_i\cdot(\mathbf{v}_{ji}\times\boldsymbol{\zeta}_i)}{\left|\mathbf{w}_i\right|}G_i - \frac{\partial\widetilde{C}_{Li}}{\partial\alpha}\frac{v_{ai}(\mathbf{v}_{ji}\cdot\mathbf{u}_{ni}) - v_{ni}(\mathbf{v}_{ji}\cdot\mathbf{u}_{ai})}{v_{ai}^2 + v_{ni}^2} \tag{52}$$

where δ_{ij} is the Kronecker delta and

$$\begin{aligned}\mathbf{w}_i &\equiv \mathbf{u}_i\times\boldsymbol{\zeta}_i\\ v_{ni} &\equiv \mathbf{u}_i\cdot\mathbf{u}_{ni}\\ v_{ai} &\equiv \mathbf{u}_i\cdot\mathbf{u}_{ai}\end{aligned} \tag{53}$$

This solution method generally converges very rapidly to the solution. However, it requires an initial guess for the vortex strengths. An initial guess can be obtained by applying the small angle approximation to the system of equations and linearizing the system.

For small angles of attack, the section lift coefficient can be expressed as

$$\widetilde{C}_{Li} = \frac{\partial\widetilde{C}_{Li}}{\partial\alpha}(\alpha_i - \alpha_{L0i} + \varepsilon_i\delta_i) \tag{54}$$

The angle of attack at any control point is the sum of the freestream angle of attack and the induced angle of attack

$$\alpha_i = \alpha_\infty + \alpha_{\text{ind},i} = \tan^{-1}\left(\frac{\mathbf{u}_\infty \cdot \mathbf{u}_{ni}}{\mathbf{u}_\infty \cdot \mathbf{u}_{ai}}\right) + \tan^{-1}\left(\frac{\sum_{j=1}^{2n} G_j \mathbf{v}_{ji} \cdot \mathbf{u}_{ni}}{\sum_{j=1}^{2n} G_j \mathbf{v}_{ji} \cdot \mathbf{u}_{ai}}\right) \quad (55)$$

Using the small angle approximation for the induced angle of attack gives an initial guess for the local angle of attack

$$\alpha_i = \tan^{-1}\left(\frac{\mathbf{u}_\infty \cdot \mathbf{u}_{ni}}{\mathbf{u}_\infty \cdot \mathbf{u}_{ai}}\right) + \sum_{j=1}^{2n} G_j \mathbf{v}_{ji} \cdot \mathbf{u}_{ni} \quad (56)$$

Using Eq. (56) in Eq. (54) gives

$$\widetilde{C}_{Li} = \frac{\partial \widetilde{C}_{Li}}{\partial \alpha}\left[\tan^{-1}\left(\frac{\mathbf{u}_\infty \cdot \mathbf{u}_{ni}}{\mathbf{u}_\infty \cdot \mathbf{u}_{ai}}\right) + \sum_{j=1}^{2n} G_j \mathbf{v}_{ji} \cdot \mathbf{u}_{ni} - \alpha_{L0i} + \varepsilon_i \delta_i\right] \quad (57)$$

Using this expression for the lift coefficient in Eq. (46) and dropping second-order terms gives a linear approximation for the solution

$$2|\mathbf{u}_\infty \times \boldsymbol{\zeta}_i| G_i - \frac{\partial \widetilde{C}_{Li}}{\partial \alpha} \sum_{j=1}^{2n} G_j \mathbf{v}_{ji} \cdot \mathbf{u}_{ni} = \frac{\partial \widetilde{C}_{Li}}{\partial \alpha}\left[\tan^{-1}\left(\frac{\mathbf{u}_\infty \cdot \mathbf{u}_{ni}}{\mathbf{u}_\infty \cdot \mathbf{u}_{ai}}\right) - \alpha_{L0i} + \varepsilon_i \delta_i\right] \quad (58)$$

which can easily be solved for use as an initial guess to the nonlinear system of equations.

IV. Aerodynamic Forces and Moments

Once the vortex strengths are known, the total aerodynamic force and moment on the aircraft can be found by summing the aerodynamic force and moment contributed by each horseshoe vortex sheet. The total aerodynamic force is the summation of the aerodynamic force from each horseshoe vortex sheet

$$\frac{\mathbf{F}}{\frac{1}{2}\rho V_\infty^2 S_r} = \sum_{k=1}^{n} \mathbf{f}_k \quad (59)$$

and the total aerodynamic moment is the summation of the aerodynamic moment from each horseshoe vortex sheet

$$\frac{\mathbf{M}}{\frac{1}{2}\rho V_\infty^2 S_r L_r} = \sum_{k=1}^{n} \mathbf{m}_k \quad (60)$$

In the development of this method, we have assumed that the vorticity varies linearly along the bound segment of the horseshoe vortex sheet. If we also assume that the induced velocity along the sheet varies linearly, the local vorticity and local velocity along the bound segment of the horseshoe vortex sheet can be written as

$$\Gamma = \Gamma_a + (\Gamma_b - \Gamma_a)\zeta \quad (61)$$

$$\mathbf{V} = \mathbf{V}_a + (\mathbf{V}_b - \mathbf{V}_a)\zeta \quad (62)$$

Using these expressions in Eq. (35) gives an expression for the differential force vector along a differential segment of the bound vortex segment

$$\mathbf{dF} = \rho[\Gamma_a + (\Gamma_b - \Gamma_a)\zeta][\mathbf{V}_a + (\mathbf{V}_b - \mathbf{V}_a)\zeta] \times \mathbf{dl} \quad (63)$$

Applying the change of variables given in Eq. (4) to Eq. (63) and integrating along the length of the bound vortex segment of horseshoe vortex k gives

$$\begin{aligned}\mathbf{F}_k &= \rho \int_{\zeta=0}^{1} [\Gamma_{a_k} + (\Gamma_{b_k} - \Gamma_{a_k})\zeta][\mathbf{V}_{a_k} + (\mathbf{V}_{b_k} - \mathbf{V}_{a_k})\zeta] \times \boldsymbol{l}_k d\zeta \\ &= \rho\{\Gamma_{a_k}\mathbf{V}_{a_k} + \tfrac{1}{2}[(\Gamma_{b_k} - \Gamma_{a_k})\mathbf{V}_{a_k} + \Gamma_{a_k}(\mathbf{V}_{b_k} - \mathbf{V}_{a_k})] \\ &\quad + \tfrac{1}{3}(\Gamma_{b_k} - \Gamma_{a_k})(\mathbf{V}_{b_k} - \mathbf{V}_{a_k})\} \times \boldsymbol{l}_k\end{aligned} \quad (64)$$

The strength of the bound vortex at the corners $\mathbf{P}_a$ and $\mathbf{P}_b$ is related to the strength of the bound vortex at control points $\mathbf{P}_1$ and $\mathbf{P}_2$ as shown in Eq. (9). Likewise, the velocities at these points are related according to

$$\begin{aligned}\mathbf{V}_{a_k} &= \mathbf{V}_{1_k}\left(1 + \frac{\sigma_{1_k}}{\sigma_{2_k} - \sigma_{1_k}}\right) - \mathbf{V}_{2_k}\left(\frac{\sigma_{1_k}}{\sigma_{2_k} - \sigma_{1_k}}\right) \\ \mathbf{V}_{b_k} &= \mathbf{V}_{1_k}\left(1 - \frac{1 - \sigma_{1_k}}{\sigma_{2_k} - \sigma_{1_k}}\right) + \mathbf{V}_{2_k}\left(\frac{1 - \sigma_{1_k}}{\sigma_{2_k} - \sigma_{1_k}}\right)\end{aligned} \quad (65)$$

Using Eqs. (32) and (65) in Eq. (64) gives the aerodynamic force from one horseshoe vortex sheet. In nondimensional form, it can be written as

$$\begin{aligned}\mathbf{f}_k &\equiv \frac{\mathbf{F}_k}{\frac{1}{2}\rho V_\infty^2 S_r} \\ &= -\frac{\cos\Lambda_k l_k}{S_r}\boldsymbol{\zeta}_k \times [2G_{a_k} c_{a_k} \mathbf{u}_{a_k} \\ &\quad + (G_{b_k} c_{b_k} - G_{a_k} c_{a_k})\mathbf{u}_{a_k} + G_{a_k} c_{a_k}(\mathbf{u}_{b_k} - \mathbf{u}_{a_k}) \\ &\quad + \tfrac{2}{3}(G_{b_k} c_{b_k} - G_{a_k} c_{a_k})(\mathbf{u}_{b_k} - \mathbf{u}_{a_k})]\end{aligned} \quad (66)$$

where

$$G_{a_k} \equiv G_{1_k}\left(1+\frac{\sigma_{1_k}}{\sigma_{2_k}-\sigma_{1_k}}\right)-G_{2_k}\left(\frac{\sigma_{1_k}}{\sigma_{2_k}-\sigma_{1_k}}\right)$$
$$G_{b_k} \equiv G_{1_k}\left(1-\frac{1-\sigma_{1_k}}{\sigma_{2_k}-\sigma_{1_k}}\right)+G_{2_k}\left(\frac{1-\sigma_{1_k}}{\sigma_{2_k}-\sigma_{1_k}}\right) \quad (67)$$

$$\mathbf{u}_{a_k} \equiv \mathbf{u}_{1_k}\left(1+\frac{\sigma_{1_k}}{\sigma_{2_k}-\sigma_{1_k}}\right)-\mathbf{u}_{2_k}\left(\frac{\sigma_{1_k}}{\sigma_{2_k}-\sigma_{1_k}}\right)$$
$$\mathbf{u}_{b_k} \equiv \mathbf{u}_{1_k}\left(1-\frac{1-\sigma_{1_k}}{\sigma_{2_k}-\sigma_{1_k}}\right)+\mathbf{u}_{2_k}\left(\frac{1-\sigma_{1_k}}{\sigma_{2_k}-\sigma_{1_k}}\right) \quad (68)$$

Equation (66) can be used in Eq. (59) to calculate the net aerodynamic force on the aircraft.

The differential aerodynamic moment caused by the differential force from a differential length along the bound vortex of a horseshoe vortex sheet about the center of gravity can be written as the force crossed with the distance of the force from the center of gravity, $\mathbf{r}_{CG}$

$$\mathbf{dM} = \mathbf{r}_{CG} \times (\rho \Gamma \mathbf{V} \times \mathbf{d}\boldsymbol{l}) \quad (69)$$

Again assuming that the vorticity and velocity vary linearly along the bound vortex as does the distance to the center of gravity and applying the change of variables given in Eq. (4)

$$\mathbf{dM} = [\mathbf{r}_{CG_a} + (\mathbf{r}_{CG_b} - \mathbf{r}_{CG_a})\zeta] \times \{\rho[\Gamma_a + (\Gamma_b - \Gamma_a)\zeta][\mathbf{V}_a + (\mathbf{V}_b - \mathbf{V}_a)\zeta] \times \boldsymbol{l} d\zeta\} \quad (70)$$

This can be integrated and the result used in Eq. (60). If this work is pursued further, this expression will be obtained and reported in a future publication. However, it does not affect the results included in this work and will not be included here.

V. Results

The work presented here provides two methods for evaluating the influence of a vortex sheet on a control point located along the bound portion of the horseshoe vortex sheet. Because the influence is indeterminate when the sheet has some component of sweep, either the sheet influence on a control point located along the bound vortex must be ignored, or the sheet influence can be assumed to be the influence of a similar sheet having no sweep or dihedral. In the results that follow, those results titled "With Sheet" include the effects of a sheet with no sweep and dihedral as given in Eq. (29). Those results titled "Without Sheet" are equivalent to setting $\mathbf{v}_s = 0.0$ when the influence of a sheet must be evaluated at a point located along the bound portion of the sheet.

Using Prandtl's classical lifting-line theory, a closed-form solution for lift on an elliptic wing can be obtained. This provides a good candidate for assessing the accuracy of numerical lifting-line methods. An elliptic wing shown in Fig. 7 of aspect ratio $32/\pi$ with a lift slope of 2π was used for comparison of the lifting-line methods. Fig. 8 shows the lift coefficient for the elliptic wing at 5 degrees angle of attack as predicted by the two methods obtained from this work as well as the work by Phillips and Snyder as a function of the number of elements used to discretized the wing. Note that all three methods appear to converge to the correct solution. However, the method of Phillips and Snyder in general has less error than the methods used in this work.

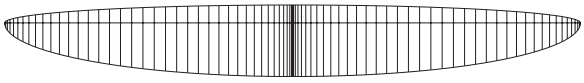

Figure 7. Elliptic wing of aspect ratio $32/\pi$.

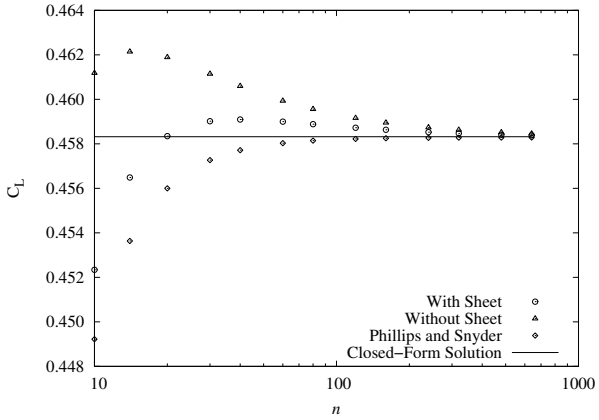

Figure 8. Lift Coefficient as a function of number of discretization elements for an elliptic wing with aspect ratio $32/\pi$.

Figure 9 shows the same data as that in Figure 8, but plotted to show the percent error between the exact solution and that predicted by each of the methods. Notice that the method of Phillips and Snyder does in fact have significantly lower error than the other methods for low grid resolution. However, the method of Phillips and Snyder does not fully converge to the correct solution. From the data presented here, it appears that one or both of the methods developed in this work may fully converge to the correct solution, although the methods would need to be run at higher grid resolutions to confirm this.

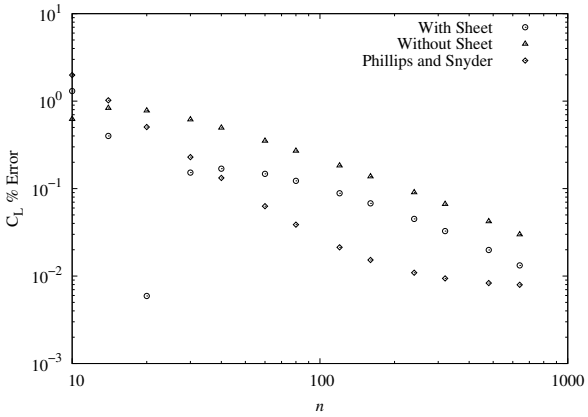

Figure 9. Percent error of the lift coefficient as a function of grid resolution.

As a final comment on Fig. 9, note that the order of convergence of the horseshoe vortex sheet methods does not seem to offer any improvement to the order of convergence of the method of Phillips and Snyder. If the order of convergence were an improvement, the slope of the data in Fig. 9 from the vortex sheet methods would be greater than the slope of the data from the Phillips and Snyder method.

The behavior of the methods for wings with sweep is also of interest because Prandtl's original lifting-line method cannot be extended to wings with sweep or dihedral. The methods were used to predict the lift on a rectangular wing of aspect ratio 8 having 45 degrees of sweep as shown in Figure 10.

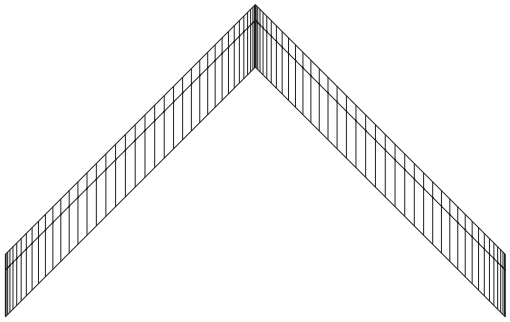

Figure 10. Rectangular wing with aspect ratio of 8 and 45 degrees of sweep.

Figure 11 shows the results of the lift coefficient predicted for this wing at 5 degrees angle of attack. Also included are results predicted by the method of Phillips and Snyder, but with a variation in the placement of the lifting line based on a modification suggested by Kuchemann[10]. A representative lifting-line distribution based on the Kuchemann modification is included in Fig. 12. Notice from Fig. 11 that *none* of these methods converge to a solution if the wing has sweep. As the grid is refined, the solutions all continue to change in what appears to be a linear manner on a log-scale plot. Originally it was assumed that this was due to the first-order discontinuity in the lifting line as it crosses the plane of symmetry of the wing. However, the modification suggested by Kuchemann eliminates this possibility because the first derivative of the lifting line for this modification is continuous across the wing plane of symmetry. From the results in Fig. 11, it must be assumed that there is something in the development of these methods that prohibits grid refinement for wings with sweep. This is a possible topic of future research.

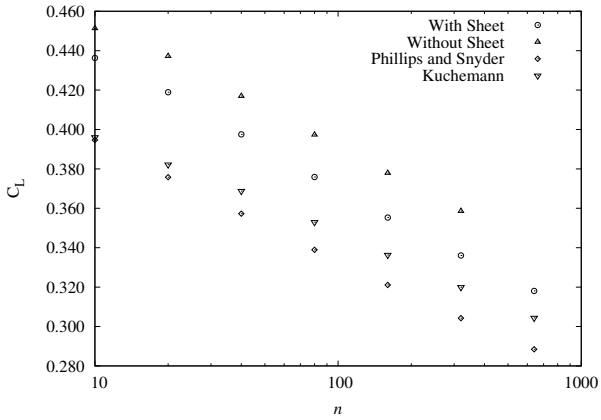

Figure 11. Lift coefficient for a wing of aspect ratio of 8 with 45 degrees of sweep as a function of grid resolution.

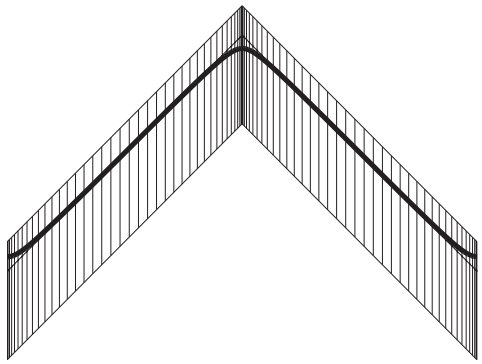

Figure 12. Lifting-line distribution based on the work of Kuchemann showing first-order continuity at wing plane of symmetry.

As a final assessment of the accuracy of the methods examined here, a system of interacting lifting surfaces was considered. This system of lifting surfaces included wings with sweep and dihedral and 20 control points per semi-span were used for the calculations. Figure 13 shows the circulation distribution along the spans of the lifting surfaces for the "With Sheet" case. Similar distributions were obtained for the "Without Sheet" case as well as the Phillips and Snyder method.

The greatest difference in the total lift coefficient as predicted from the three numerical models was 1.6%. Because aerodynamic coefficients generally cannot be measured to that accuracy, the numerical method presented in this paper provides a design tool that can be expected to give results to within experimental accuracy of those predicted by the method of Phillips and Snyder.

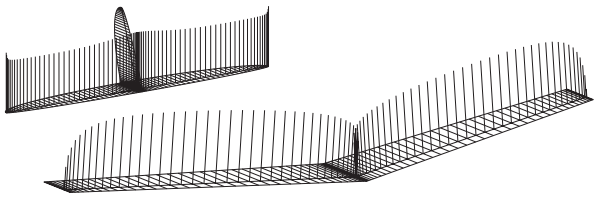

Figure 13. Circulation distribution for a system of interacting lifting surfaces.

VI. Conclusion

The definition of a horseshoe vortex sheet singularity is developed, and a numerical lifting-line method for evaluating the aerodynamic forces and moments on a system of lifting surfaces based on this singularity is presented. The velocity induced at an arbitrary point in space by the singularity can be evaluated from Eq. (30) in conjunction with either Eq. (27), (28), or (29) depending on the position of the point of interest. It was found that the velocity induced at a point along the bound portion of the horseshoe vortex sheet with sweep is singular. Two methods of circumventing this difficulty were suggested which included 1) evaluating the induced velocity along the bound portion as though the sheet were unswept, or 2) setting the induced velocity along the bound portion to zero.

In general, the numerical method produced results that agree very closely with results based on the method of Phillips and Snyder[8]. One advantage of the method can be seen in the evaluation of the aerodynamic properties of a wing with no sweep and no dihedral. For wings with no sweep or dihedral, the method produced results that grid resolve to accurate solutions which may be more accurate than those of Phillips and Snyder. For wings with sweep and/or dihedral, the method does not produce grid-resolved results which was also found to be the case with the method of Phillips and Snyder.

The results show that the vortex sheet method presented here has apparent drawbacks. First, the method appeared to require higher grid resolution to match the accuracy of previous methods. Second, it did not seem to improve the order of convergence over zeroth-order methods. Finally, evaluating the influence of a vortex sheet on an arbitrary point in space is generally more computationally expensive than other methods based on lifting-line theory because this method requires numerical integration for points not collinear with the bound segment of the horseshoe vortex sheet.

Future work may include using the method to evaluate the aerodynamic center of wings with sweep and dihedral. Common numerical lifting-line methods fail to accurately predict the location of the aerodynamic center of wings, and if the method presented here could improve such estimations, the aerodynamic center predicted by this method would be of interest.

The singularities used in this work do not weaken with grid refinement. This is likely the root problem that grid resolved solutions could not be obtained for wings with sweep and/or dihedral. Fundamentally, future research should be focused on a numerical lifting-line method that weakens singularities with grid refinement.

References

[1]Prandtl, L., "Tragflügel Theorie," *Nachrichten von der Gesellschaft der Wisseschеaften zu Göttingen*, Geschäeftliche Mitteilungen, Klasse, 1918, pp. 451 – 447.

[2]Prandtl, L., "Applications of Modern Hydrodynamics to Aeronautics," NACA 116, June 1921.

[3]Kutta, M. W., "Auftriebskräfte in Strömenden Flüssigkeiten," *Illustrierte Aeronautische Mitteilungen*, Vol. 6, 1902, p. 133.

[4]Joukowski, N. E., "Sur les Tourbillons Adjionts," *Traraux de la Section Physique de la Societe Imperiale des Amis des Sciences Naturales*, Vol. 13, No. 2, 1906.

[5]McCormick, B. W., "The Lifting Line Model," *Aerodynamics, Aeronautics and Flight Mechanics*, 2nd ed., Wiley, New York, 1995, pp. 112 – 119.

[6]Anderson, J. D., Jr., Corda, S., and Van Wie, D. M., "Numerical Lifting-Line Theory Applied to Drooped Leading-Edge Wings Below and Above Stall," *Journal of Aircraft*, Vol. 17, No. 12, 1980, pp. 898 – 904.

[7]Katz, J., and Plotkin, A., "Lifting-Line Solution by Horseshoe Elements," *Low-Speed Aerodynamics, from Wing Theory to Panel Methods*, McGraw-Hill, New York, 1991, pp. 379 – 386.

[8]Phillips, W. F., and Snyder, D. O., "Modern Adaption of Prandtl's Classic Lifting-Line Theory," Journal of Aircraft, Vol. 37, No. 4, 2000, pp. 662 – 670.

[9]Saffman, P. G., "Vortex Force and Bound Vorticity," *Vortex Dynamics*, Cambridge Univ. Press, Cambridge, England, U.K., 1992, pp. 46 – 48.

[10]Kuchemann, D., "A Simple Method for Calculating the Span and Chordwise Loading on Straight and Swept Wings of any Given Aspect Ratio at Subsonic Speeds," Aeronautical Research Council, RM-2935, London, May, 1956.